Biomedical Microdevices (2025) 27:24
https://doi.org/10.1007/s10544-025-00754-1

RESEARCH

Small form factor implantable neural probe with efficient flip chip µLED for in vivo optogenetics

Mafalda Abrantes[1,2,3] · Tiago Pereira[1,2] · Patrícia Silva[1,4] · Margarida Falcão[1,4] · Jérôme Borme[2] · Pedro Alpuim[2,3] · Luis Jacinto[1,4]

Accepted: 14 May 2025

Abstract
Optogenetics is a widely used tool to dissect neural circuits with optical stimulation, but it requires that light is delivered to photosensitive neurons inside the brain. Implantable neural probes with microscale LEDs (µLEDs) are an emerging approach to delivering light to the brain with superior light output control. However, approaches to integrate µLEDs in neural probes depend on complex fabrication processes. Here, we developed an implantable small form factor neural probe that integrates highly efficient commercial flip chip µLEDs using only standard lithography processes in silicon and a custom automated LED mounting approach with custom 3D-printed tools on a pick-and-place machine. The probe has a cross-sectional area under 0.013 mm^2 but can output up to 2.5 mW of optical power with an irradiance of 175 mW/mm^2. Due to the high plug efficiency of the LED, the neural probe can perform stimulation protocols up to 20 Hz and 80% duty cycles without surpassing estimated hotspot temperature elevations above 1 ºC. The neural probes were validated in vivo, with brain activity in the motor cortex of transgenic mice being reliably modulated by pulsed light emitted from the probe.

Keywords µLED · MEMS · Neural probe · Optogenetics · Neurostimulation · Photonics · Optoelectronics

1 Introduction

Optogenetics is a powerful tool to modulate neuronal circuits with optical stimulation and it has been widely used to dissect functional connections in the brains of preclinical animal models (Yizhar et al. 2011; Bernstein and Boyden 2011; Tye and Deisseroth 2012). Through the genetic modification of neuronal cells under the control of specific promoters to express light-gated channels and pumps, optogenetics allows selective excitation and inhibition of neuronal circuits with millisecond resolution using different light wavelengths (Fenno et al. 2011; Zeng and Madisen 2012). This has allowed researchers to map functional connections between different cell types in brain circuits or between different brain areas, as well as to highlight potential cellular targets for brain disorders (Tye and Deisseroth 2012; Chen et al. 2022; Deisseroth 2014). Initial approaches to deliver light inside the brain to activate photosensitive cells resorted to implantable optical fibers connected to an external light source such as a laser or an LED (Warden et al. 2014). These systems were widely disseminated as they are easily scalable and optical fiber implants are simple to fabricate. Over the past decade, advances in optoelectronics, photonics, and microfabrication processes led to alternative approaches in which the light source could be implanted inside the brain (Chen et al. 2024; Barros and Cunha 2024; Xu et al. 2023). This can be achieved, for example, by the integration of microscale LEDs (µLEDs) in micron-size implantable neural probes using silicon-based MEMS fabrication techniques similar to the ones already used for developing neural probes for electrophysiological recordings (Chen et al.

Mafalda Abrantes and Tiago Pereira contributed equally to this work.

✉ Luis Jacinto
ljacinto@med.up.pt

1 Department of Biomedicine – Experimental Biology Unit, Faculty of Medicine, University of Porto (FMUP), Porto 4200-319, Portugal

2 International Iberian Nanotechnology Laboratory, Braga 4715-330, Portugal

3 Centro de Física das Universidades do Minho e Porto, University of Minho, Braga 4710-057, Portugal

4 Rise-Health - Department of Biomedicine, Faculty of Medicine, University of Porto (FMUP), Porto 4200-319, Portugal

Published online: 29 May 2025

2024; Qazi et al. 2018). Neural probes with µLEDs allow direct light output control with low operational currents and voltages, facilitating multiplexed array designs, wireless operation, and integration in multifunctional devices (Qazi et al. 2018; Silva and Jacinto 2025), and open new pathways for optical interrogation of neural circuits.

The integration of µLEDs in neural probes for optogenetics can follow different routes, each with advantages and disadvantages. One route resorts to monolithic integration by fabricating the device directly on sapphire or silicon epitaxial wafers with gallium nitride (GaN) (Wu et al. 2015; Scharf et al. 2016; Reddy et al. 2019). This option offers limited substrate choices and can bring additional compromises regarding materials and processes (Chen et al. 2024; Goncalves et al. 2017). Because the entire wafer is used for device fabrication, a cumbersome thinning step is often necessary to reduce the probe's final implant footprint (Wu et al. 2015; Reddy et al. 2019). Another route consists of epitaxial lift-off from wafers with GaN followed by transfer printing to a target substrate such as silicon (Ayub et al. 2020) or polyimide (Il Kim et al. 2013; Li et al. 2022). This approach retains the optoelectronic performance of µLEDs grown on the epitaxial wafers and introduces fabrication flexibility of the final device, including in the choice of substrates that can then be released to create smaller cross-section or flexible neural probes (Il Kim et al. 2013; Li et al. 2022). However, the transfer and bonding steps to the target wafer can be complex, requiring temporary handling wafers or assistive transfer support materials and post-transfer processing steps. Both routes can produce very thin µLEDs (< 5 µm) integrated into reduced thickness neural probes (15–120 µm) but typically suffer from low wall-plug efficiency (< 1–2%) and low optical power and irradiance.

An alternative route is the integration of commercially available small-footprint flip chip µLEDs, that were produced for other applications, through micrometric positioning and bonding to appropriate bonding pads fabricated on the probe's substrate. But placing and effectively bonding and passivating the chips can be challenging due to their small size and the reduced dimensions of the implantable shanks in the neural probes. Previous approaches have mainly used large area µLEDs (> 0.06 mm^2) and thicker substrates (up to 700 µm) that can withstand the post-fabrication mounting and bonding processes to overcome such difficulties (Il Park et al. 2016; Shin et al. 2017; Fan et al. 2016; Ayub et al. 2017). The result is neural probes with large cross-sectional areas, potentially leading to more tissue damage upon implantation and poor performance.

In addition to the implant footprint, another concern with implantable neural probes with µLEDs is that a large portion of the input power is converted into heat, not optical power (Dong et al. 2018). Temperature elevations in brain tissue can have modulatory effects on neuronal cell activity or even cause tissue damage (Yizhar et al. 2011; Dong et al. 2018; Owen et al. 2019). Although there are no official guidelines specific to brain implants, regulations limit surface temperature rises of implantable medical devices to 2 ºC. To stay on the conservative side, there is acceptance that µLED neural probes should not increase brain tissue temperature by more than 1 ºC during operation (Dong et al. 2018). Due to the low wall-plug efficiency of µLEDs used in neural probes and the necessity of using higher voltages to achieve reliable turn-on currents, most neural probes with µLEDs are limited to operation with either low driving currents or low frequency and duty-cycle stimulation protocols to avoid unintended temperature elevations above the 1 ºC limit.

Here, we report on an implantable silicon-based neural probe that integrates highly efficient small-sized commercial bare die µLEDs on thin shanks with a small final cross-section and high optical output power. A custom method was developed to mount, bond, and passivate the µLEDs on 15 µm-thin probe shanks using custom-printed 3D tools on a pick-and-place machine. The final cross-sectional area of the probe is only 0.013 mm^2, which is significantly smaller than that of the smallest optical fiber implants used in mice. The probe can output up to 2.3 mW of optical power with an irradiance of 175 mW/mm^2, with approximately 15% plug-efficiency while maintaining hotspot temperature elevation below 1 ºC for frequencies up to 20 Hz and duty cycles below 80%. The probe was validated in vivo by driving opto-evoked activity in the motor cortex of transgenic mice.

2 Methods

2.1 Neural probe fabrication

A standard silicon-on-insulator (SOI) wafer (15 µm silicon (Si) / 2 µm silicon dioxide (SiO_2) / 650 µm Si / 2 µm SiO_2) (Silicon Valley Microelectronics) was used (Fig. 1a). The fabrication process started with the sputtering of an alumina insulator film (Al_2O_3, 100 nm) on the front side of the wafer, and the deposition of 1500 nm of SiO_2 on the back side by plasma-enhanced chemical vapor deposition (PECVD) (Fig. 1b, c). Then, a 5 nm layer of chromium (Cr), as adhesion for the gold (Au) contact layer, and 200 nm of Au were sputtered on the front side (Fig. 1d). Probe contacts, pads, and conductive lines were patterned by photolithography and etched by ion milling (Fig. 1e, f). On the back side, a SiO_2 hard mask was patterned by reactive ion etching to define the regions that would later be etched up to the device layer (Fig. 1g, h). A layer of 200 nm of Al_2O_3 was deposited on the front side by atomic layer deposition (ALD) for device

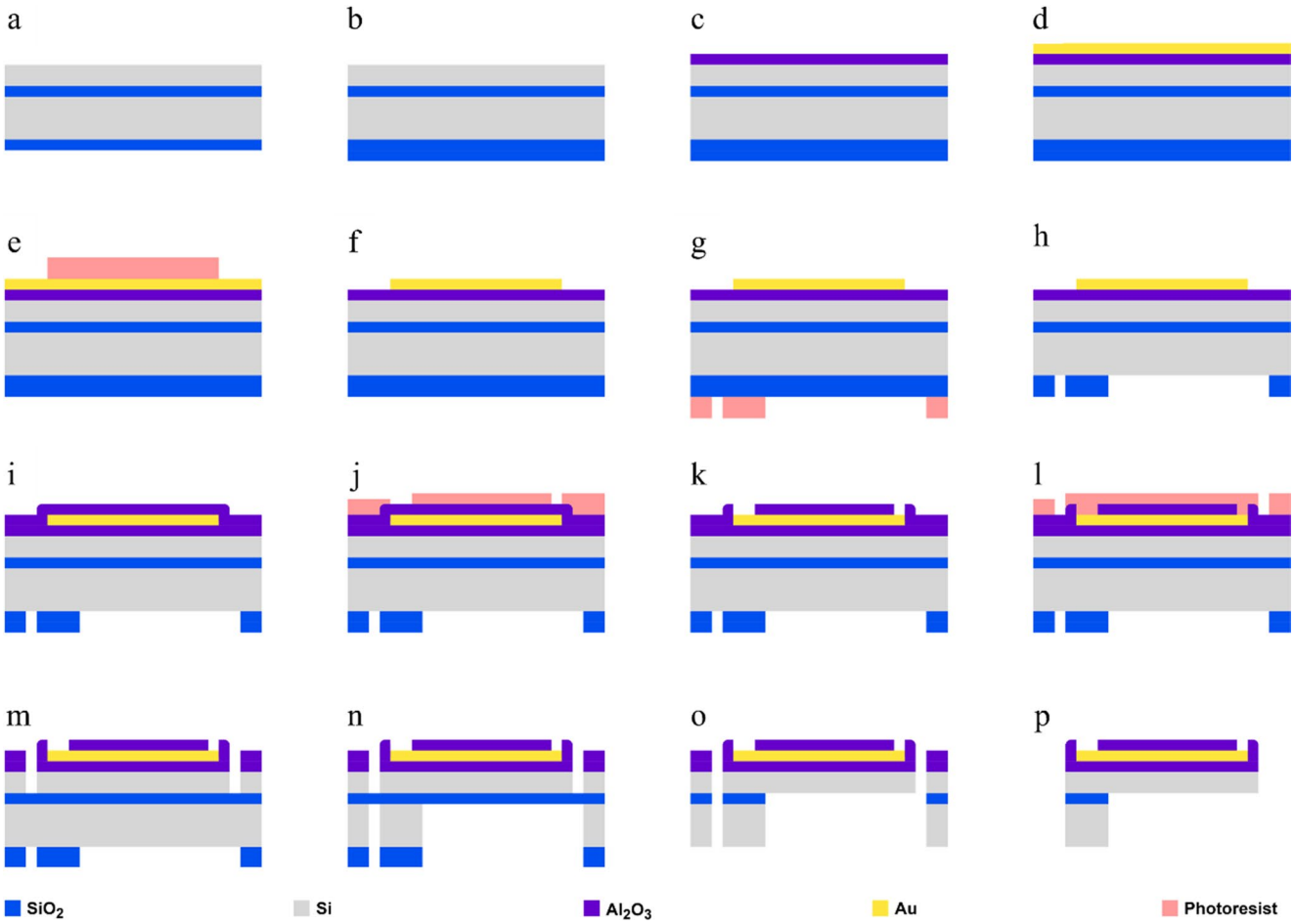

Fig. 1 Neural probe fabrication process. (**a**) Silicon-on-insulator (SOI) wafer. (**b**) Back-side silicon oxide (SiO_2) layer deposition. (**c**) Top-side alumina (Al_2O_3) layer deposition. (**d-f**) Gold (Au) deposition and patterning of interconnect lines and bonding pads. (**g-h**) Back-side SiO_2 patterning. (**i-k**). Top-side Al_2O_3 passivation and patterning of bonding and connector pads. (**l-m**) Top-side etching to define probe layout. (n) Backside etching to define probe layout and remove silicon (Si) from under the neural probe shank. (**o**) SiO_2 etching to release device layer. (**p**) Final released neural probe. NB: not to scale

passivation, and probe contacts and pads were exposed by ion milling (Fig. 1i, j,k). The outline of each probe was defined by photolithography, and the wafer's Si device layer (15 µm) was etched by deep reactive ion etching (DRIE) (Fig. 1l.m). Then, the back side of the wafer (Si 650 µm) under the probe's shank was etched with the same DRIE process until the buried 2 µm SiO_2 layer was reached (Fig. 1n). Finally, the buried oxide layer of the neural probe shank was etched by hydrogen fluoride (HF) vapor (Fig. 1o, p). Probes were released from the wafer by breaking two thin silicon bridges that connected the probes' base to the wafer.

2.2 µLED integration in neural probe

µLEDs (UB06 FP2, Light Avenue) were mounted on the neural probe shank by a pick-and-place system (Fineplacer Sigma, Finetech) with custom-designed holders and tips. A specially designed holder for handling the probe during the process was printed on a stereolithography resin 3D printer (Form 3+, Formlabs) and cured by ultra-violet (UV) light exposure (in Form Cure, Formlabs). Double-sided thermal-release tape (TRT) was taped to the holders to attach the probe's shanks. Probes were inserted into the holders with the help of tweezers and, after vacuum fixation in the pick-and-place working stage, these were gently pressed (0.02 N) against the TRT with a custom 3D printed tip tool (with a cylinder tip of 500 µm diameter). Conductive adhesive (Ablestick ABP 8037 TI, Loctite) was stamped on each probe's bonding pad with another stamping tool (150 µm diameter semisphere DAUB tip, Small Precision Tools). Then, the µLEDs were positioned on the pads with a pick-and-place vacuum tool (2-sided Inverted Channel Die Collect, Small Precision Tools) and baked in a furnace to cure the conductive adhesive with a 30 min temperature ramp between 25° C and 160 °C, followed by 45 min at 160 °C. After cooling to room temperature, the µLEDs on the probes' shanks were

passivated with a thin 5–10 µm layer of acrylic-based transparent coating for optical applications (8424 UV, IQ-BOND) with a custom pick-and-place 3D printed tool. Finally, the coating was cured with UV-light exposure for 5 s.

2.3 µLED neural probe packaging

The µLED probes were packaged with a custom-designed PCB (5.9 × 6 × 0.8 mm) with electroless nickel immersion gold (ENIG) finishing. Probe connector pads were wire-bonded to PCB pads with 25 µm gold wire in a wire bonder (HB16, TPT), and a connector (853-93-100-10-001000, Mill-Max Mfg. Corp.) was soldered to the PCB.

2.4 Electrical and optical characterization

I-V characterization was performed with a source meter unit (2400 SourceMeter, Keithley) connected to the probe's PCBs with tungsten probes. Voltage sweeps from 2.5 V to 3.2 V were applied with 0.1 V increments, with current limited to 6 mA. Optical output was measured in the same setup by placing a photodiode power sensor (S121 C, Thorlabs) above the µLED at approximately 1 mm and connected to a power meter (PM101, Thorlabs). One µLED neural probe was immersed in phosphate-buffered saline (PBS) solution for 12 days, and the current was measured daily to a forward bias of 2.8 V to assess the passivation coating efficiency.

2.5 Thermal modeling

Heat transfer simulations were modelled in COMSOL Multiphysics (COMSOL Inc) using the Heat Transfer module. The model consisted of a probe with a body assumed to be silicon (density $\rho = 2329$ kg m^{-3}, heat capacity $CP = 700$ J kg^{-1} K^{-1}, thermal conductivity $k = 130$ W m^{-1} K^{-1}) and with the same geometry as the fabricated neural probes. At the tip of the probe's shank, two blocks with an area of 89 × 150 μm^2 were stacked to mimic the µLED geometry. The bottom and top blocks were assumed to be SiC (density $\rho = 3216$ kg m^{-3}, heat capacity $CP = 490$ J kg^{-1} K^{-1}, thermal conductivity $k = 690$ W m^{-1} K^{-1}) and sapphire (density $\rho = 3980$ kg m^{-3}, heat capacity $CP = 800$ J kg^{-1} K^{-1}, thermal conductivity $k = 45$ W m^{-1} K^{-1}), with 30 µm and 50 µm thickness, respectively, adding up to the 80 µm µLED's total thickness. A thin 10 µm thick layer of PMMA (density $\rho = 1200$ kg m^{-3}, heat capacity $CP = 1446$ J kg^{-1} K^{-1}, thermal conductivity $k = 0.193$ W m^{-1} K^{-1}) surrounding the two µLED blocks was modelled to simulate the transparent acrylic-based coating. The shank was assumed to be inside brain tissue (density $\rho = 1040$ kg m^{-3}, heat capacity $CP = 3650$ J kg^{-1} K^{-1}, thermal conductivity $k = 0.527$ W m^{-1} K^{-1}) with the bulk of the probe being in air (COMSOL's model). Outside and brain temperature were initially defined at 21 °C and 37 °C, respectively. Heating was assumed to originate from the walls of the SiC block and the top surface of the probe's shank and modelled by applying Boundary Heat Sources to its faces. A time-dependent simulation was run in 1 ms time intervals from 0 to 1 s. Output power was assumed to be due to Joule Heating in the probe's shank ($P = RI^2$) and the difference of input electrical power and output optical power at the µLED ($P = V_{\mu LED}I - P_{optical}$). Tissue temperature for graphical representations was considered as the average tissue temperature in a 30 µm line from µLED coating surface.

2.6 In vivo testing

A custom tetrode device (Machado et al. 2020) carrying four nichrome tetrodes was used for electrophysiological recordings. Briefly, tetrodes were prepared by twisting four 12.5 µm nichrome wires (Kanthal) with Twister3 (Newman et al. 2020) and mounted on the tetrode device with UV-cure epoxy. Following tetrodes connection to the pads with gold pins (Neuralynx), the tips of the tetrodes were cut and gold-plated as in (Machado et al. 2020). The µLED neural probe connected to the PCB package was then glued to the tetrode device with UV-cure epoxy so that the µLED was facing the tetrodes' tips at a distance lower than 1 mm.

One Emx1-Cre:Ai27D male mouse was used for in vivo tests. Mice were obtained by crossing homozygous Emx1-IRES-cre mice with homozygous Ai27D mice (JAX stocks #005628, #012567) (Gorski et al. 2002; Madisen et al. 2012). The animal was anesthetized by intraperitoneal injection of ketamine (75 mg/Kg) and medetomidine (1 mg/Kg) mix and securely placed in a stereotaxic frame (World Precision Instruments). The tetrodes and µLED neural probe assembly was lowered into the motor cortex (1.7 mm AP and 1.0 mm ML from bregma) to a depth of 0.9 mm (DV) from the brain surface. A stainless-steel screw at the back of the skull served as ground. Extracellular neuronal activity was acquired at 30 kS/s with a headstage (RHD 32ch, Intan) connected to the tetrode device and an Open Ephys acquisition system (Siegle et al. 2017), and filtered between 0.3 and 6 kHz. To evoke neuronal activity from motor cortex neurons expressing channelrhodopsin, the µLED neural probe was powered by two AA batteries at 2.7 V and controlled by an Arduino UNO (rev3, Arduino) to deliver 10 Hz light stimulation pulses (80% duty cycle). The inter-trial interval was 30 s. The Arduino also sent a 3.3 V TTL pulse during stimulation to the acquisition system for synchronization with the electrophysiological recordings. Evoked electrophysiological responses by optical stimulation were analyzed with custom matlab code. Spikes were detected if crossing an amplitude threshold five times higher than the signal's root mean square (RMS). Detected spikes were averaged in 200 ms bins for the peristimulus time histogram (PSTH).

3 Results and discussion

3.1 Probe design and fabrication

A small cross-sectional area neural probe with an integrated flip chip µLED that provides high optical power at low driving power was developed in this work for in vivo optogenetics applications. Neural probes were fabricated with standard photolithographic processes on a silicon-on-insulator (SOI) wafer (Fig. 2a, b), and the µLED chip was then transferred to the released probes post-fabrication. A SOI wafer was chosen because it allows precise etching of its bottom side to create neural probes with reduced thickness implantable shanks (device layer) and a connector section at full-wafer thickness for safe handling (Novais et al. 2021; HajjHassan et al. 2008). Probes of 3 and 6 mm lengths were fabricated to allow targeting of different cortical and subcortical brain areas in both rats and mice (Fig. 2c). The implantable

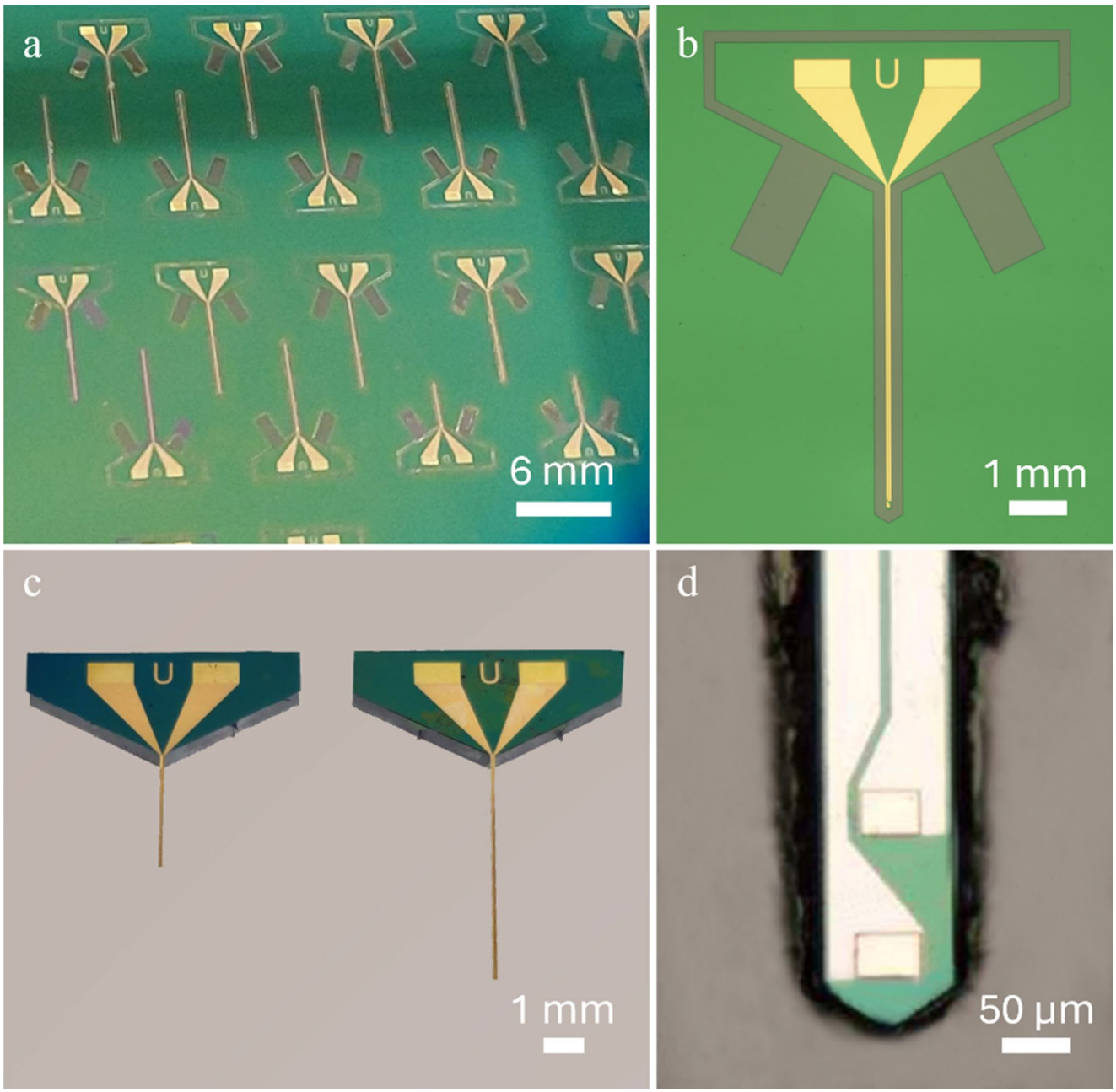

Fig. 2 Fabricated neural probes. (**a**) Detail of SOI wafer with neural probes during the fabrication process. (**b**) Optical microscopy photograph of a neural probe on wafer. (**c**) Two neural probes released from the wafer, with 3 and 6 mm implantable shanks (left and right, respectively), ready for the µLED integration process. (**d**) Optical microscopy photograph of neural probe shank's tip on wafer before the final backside etch for release, showing the wide interconnect lines and the two bonding pads for µLED mounting

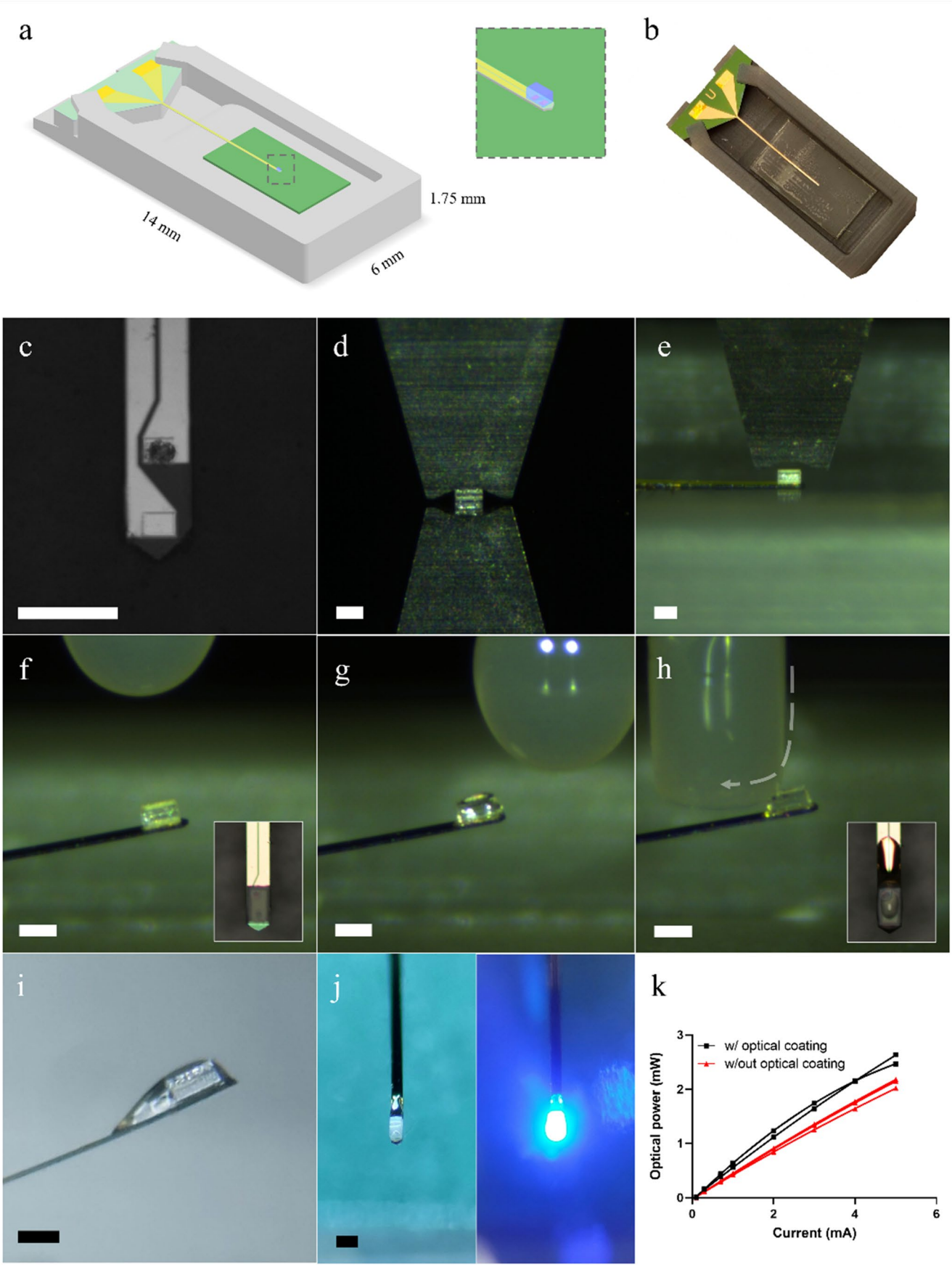
a
14 mm
6 mm
1.75 mm
b
c
d
e
f
g
h
i
j
k
w/ optical coating
w/out optical coating
Optical power (mW)
Current (mA)
0
1
2
3
0
2
4
6

Fig. 3 µLED integration on neural probe. (**a**) Schematic of custom 3D-printed probe holder with an inserted probe. The green patch under the probe's shank corresponds to the termal release tape (TRT). (Inset) Close-up schematic of a bonded µLED in the shank's tip. (**b**) Photograph of a 6 mm neural probe on a 3D-printed holder with TRT. (**c**) Shank's tip with the top bonding pad covered in conductive glue. (**d**) µLED picking process using the vacuum tip. (**e**) µLED placement on the shank's tip supported by the TRT on the probe holder. (**f**) Neural probe shank with bonded µLED, released from the TRT after curing. (Inset) Optical microscopy photograph with top view of the µLED in the probe after curing. (**g**) µLED after application of the optical coating applied with the custom 3D-printed tool. (**h**) Wiping excess optical coating of the µLED's top. Grey arrow denotes the tip's movement direction. (Inset) Optical microscopy photograph with top view of the µLED after the wiping process. (**i**) µLED profile photograph after the integration process. The optical coating creates a tail extending away from the tip that smoothens the probe's tip topography. (**j**) Photograph with top view of the finalized probe in a OFF (left) and ON (right) states. (**k**) Measured optical power output of µLEDs with (black lines) and without (red lines) optical coating. Scale in (c), (d), (e), (f), (h), (i) and (j) is 150 µm

portion of each probe, regardless of length, consists of a 99 µm wide and 15 µm thick shank with two gold 44 × 33 μm^2 bonding pads with a vertical pitch of 100 µm near the tip for posterior µLED integration (Fig. 3d). Both pads are connected to 40 µm wide gold interconnect lines (200 nm thick), with a lateral separation of 7.5 µm, extending to the connector section of the probe. The width of the shank was primarily determined by the width of the µLED to be mounted (89 × 150 µm), and gold interconnect lines were lithographically patterned to occupy most of the available space to reduce line resistance and improve heat dissipation. The connector section of the probe remained at wafer thickness (670 µm) and included two 990 × 490 μm^2 gold contact pads that were used to wire-bond the probe to a custom-designed PCB. The line resistance between µLED bonding pads and connector contact pads was calculated to be 25 and 50 Ω for the 3 and 6 µm length probes, respectively. The width of the interconnect lines could be reduced to include additional µLEDs in the shank, but to retain similar line resistances, the thickness of the deposited gold would have to be increased. The design of probes with multiple shanks to simultaneously target different brain areas could also be realized without changes to the overall fabrication process.

3.2 µLED integration

Integrating bare µLED chips in neural probes allows using highly efficient µLEDs but typically requires thick substrates to withstand the mounting and bonding processes primarily performed post-fabrication. In contrast to previous approaches that led to thick implantable probes (up to 700 µm) (Il Park et al. 2016; Shin et al. 2017; Fan et al. 2016), a novel method using custom 3D-printed holders and tips for a pick-and-place system was developed to integrate bare µLED chips with reduced dimensions (89 × 150 × 80 μm^3) in 15 µm thick suspended silicon neural probe shanks. When compared with other bare µLED chips previously used in neural probes, such as the TR2227 (220 × 270 × 50 μm^3, CREE) (Il Park et al. 2016; Shin et al. 2017; Ayub et al. 2017), the chosen LED for our probes has a considerably smaller footprint albeit being 30 µm thicker. The integration of the µLEDs on the neural probes had to be realized after the final fabrication step, that includes a hydrogen fluoride (HF) etch process to remove the buried oxide layer at the bottom of the shanks, because the LED chips could not withstand this process.

Custom 3D-printed holders were designed to hold the released neural probes tightly in position during the µLED bonding process (Fig. 3a, b), allowing for an accurate and reproducible process. The 3D printed pieces were designed to have two distinct areas that could accommodate the thickness differences between the probes' shanks (15 µm) and their connector portion (670 µm). Double-sided thermal release tape (TRT) was used in the holders to guarantee that the probe's shank could not move laterally and provide cushioning during the subsequent stamping and bonding procedures (Fig. 3b). Different pick-and-place tips, including custom-designed ones, were used to sequentially press the probe's shank against the TRT, stamp conductive glue on the shank's bonding pads, and position and press the µLED on top of the bonding pads (Fig. 3c, d,e). Following conductive glue cure in a furnace for 75 min, where the probes were also released from the TRT, a custom 3D-printed tool was used in the pick-and-place system to passivate the µLED with a thin layer of a UV-cured transparent optical coating (Fig. 3f, g). The custom-designed tool creates a coating fluid dome that envelops the µLED and guarantees both the coating of the LED and underfilling between the LED and the neural probe. The tool also allows the final wiping of any excess coating on top of the µLED for a uniform top layer that is only 5–10 µm thick (Fig. 3h). The wiping process also extends upward along the shank, away from the µLED, to create a coating slope that reduces the sharp topography change between the shank and the µLED (Fig. 3i). This approach is simultaneously more reproducible and more effective in maintaining a reduced probe thickness than, for example, dip coating, which has been used in previous µLED neural probes (Shin et al. 2017) but can double their total thickness (Sup. Fig. 1). An exploratory preliminary test also showed that hexamethyldisilazane (HMDS) vapor priming, which is a standard process in microfabrication for adhesion promotion between substrates and photoresists, increases the wettability of the µLEDs and improves coating distribution and underfilling with the described passivation process (Sup. Fig. 2). The full µLED mounting and passivation process had a yield of approximately

80%, with sources of error arising from mishandling the probes, misalignment of the µLEDs and the contact pads, and insufficient optical coating being applied. The necessity of handling the released probes and inserting them into the custom 3D holder led to some probes being lost due to human error. During stamping of conductive epoxy there was a risk of short-circuiting the two gold pads either by overapplying glue or by sub-optimal alignment of the stamping tool and substrate, but these occurred rarely. The suboptimal in-plane and out-of-place alignment of µLED and stamped gold pads could also lead a poor connection/adhesion, which resulted in the µLED being released from the probe during the curing of the conductive epoxy or in an open circuit. This error typically arised from picking up the µLED in a tilted position or miscalculating the alignment of the µLED holder and the probe and holder. Although these sources of errors became very infrequent once the user had gained experience with the process, typically after 20 probes, some process automation could be implemented to increase both its yield and scalability. Designing a wafer-sized custom holder, instead of individual probe holders, with pre-defined positions for the probes on the wafer would eliminate the need for human handling of the fragile probes. Furthermore, this could allow for computer vision pattern recognition to be adopted both for stamping the conductive glue and picking and placing the µLEDs at the wafer level. This type of pick-and-place automation is well established in industry for assembling micro-components in PCBs, including advanced systems capable of a higher number of degrees of freedom that could be used to prevent out-of-plane misalignments between µLED and bonding pads. The use of HMDS vapor priming, as described above, could also contribute to improving the application of the coating. The scale-up of this fabrication process extends to any type of available µLED that could fit the probe or to which the probe design could be adapted. The versatility of the process means that if smaller footprint µLEDs become available, smaller probes with similar characteristics could be fabricated with minimal process modifications.

The specific optical coating was chosen because of its optical transparency between 230 and 500 nm, which encompasses the emission wavelength of the used µLED (465 nm) (Fig. 3j), and its reported humidity resistance. To confirm that the optical coating did not reduce the optical output of the µLED, optical power was measured before and after the coating application. An increase in µLEDs optical power after passivation was observed (Fig. 3k). This was most likely due to a reduction of the solid angle emission of the LEDs, considering a planar photodetector and not an integrating sphere was used to measure optical power (if using the latter, output power between coated and uncoated LEDs was expected to be similar). The final cross-sectional area of the neural probe, considering the substrate, µLED, and coating, did not exceed 0.013 mm^2, which is not only smaller than in most µLED probes, regardless if they were monolithically fabricated or not, but also smaller than the smallest 100 µm optical fiber implants used in mice implants (having a footprint of approximately 0.050 mm^2 considering the core, cladding, and coating). Table 1 shows a comparison of our neural probe's characteristics with those that have been previously published.

3.3 Electro-optical and thermal characterization

The electrical and optical properties of the fabricated µLED neural probes were evaluated with a source meter and a photodetector on a probe station. Representative I-V curves and radiant flux as a function of current were obtained for the probes with µLEDs (Fig. 4a, b,c). Turn-on-voltage was observed at 2.6 V. The measured optical output power and calculated irradiance at driving voltages between 2.6 and 3.2 V (0.3 to 5 mA) ranged between 0.15 and 2.5 mW and 10 and 175 mW/mm^2, respectively (Fig. 4b, c). Although only 3 and 4 probes were tested to construct the representative I-V curves and radiant flux curves, respectively, the electrical and optical measurements presented very low variability across probes as can be observed by the low standard deviations (Fig. 4b, c) indicating high µLED operational stability and reproducibility of the fabrication method. The irradiances obtained were significantly higher than those reported for previous µLED-based probes at the same driving voltages/currents (Table 1). The high irradiance in our probes is due to the small emission area of the LED chip (89 × 150 μm^2) and its high wall-plug efficiency (WPE). The observed WPE of 14.6% is significantly higher than those previously reported for any µLED neural probe (Table 1), allowing our probe to output at least two orders of magnitude more optical power than most previous probes with similar currents (and with many also requiring higher operating voltages) (Scharf et al. 2016; Ayub et al. 2020; Li et al. 2022; Shin et al. 2017; Ayub et al. 2017; Shen et al. 2022).

LEDs are never 100% efficient, and a significant part of the driving power is converted to heat not contributing to the optical output (Dong et al. 2018). Because many neuronal circuit processes are temperature dependent, it is crucial to estimate or assess brain tissue temperature elevations due to hotspot temperature in the µLED during optical stimulation with different stimulation parameters typically used in optogenetics experiments (Dong et al. 2018; Owen et al. 2019). To evaluate the potential heating of brain tissue due to µLED probe operation, a model was developed in COMSOL Multiphysics (COMSOL Inc.) using the heat transfer module. The probe geometry was modeled with the exact dimensions of the fabricated neural probes and the µLED

Table 1 Comparison of different implantable neural probes with MLEDs for brain optogenetics

μLED	μLED dimensions (w x l x h) (μm)	μLED emission peak (nm)	Probe shank dimensions (w x h) (μm)	Cross-sectional area (mm^2)	μLEDs per shank	Probe substrate	Safe* max working current (mA)	Optical power at safe* current (mW)	Irrandiance at safe* current (mW/mm^2)	Peak Wall-plug efficiency (%)	Temperature below 1 ºC	In vivo testing	Ref
Commercial flip chip LED	89 × 150 × 80	465	99 × 105	0.014	1	Si	0.75	0.5	40	14.7	Below 20% duty cycles for currents up to 2.3 mA; or below 80% duty cycles for 0.75 mA	Mice, cortex M1	This work
GaN-Si	10 × 15 × 0.5	460	70 × 30	0.0021	3	Si	0.013	0.0003	5	0.8	Below 3.4 V	Mice, hippocampus CA1	(Wu et al. 2015)
GaN-Si	25 (diameter)	450	100 × 40	0.0040	16	Si	5	0.06	125	0.8	Below 10% duty cycles	Mice, cortex	(Scharf et al. 2016)
GaN-Si	310 × 41	450	220 × 100	0.022	3	Si	3.5	0.06	1	0.4	-	-	(Sung et al. 2017)
GaN-Si	22 × 22 × 5	445	800 × 15	0.012	32	Parylene C	0.0085	0.0013	-	0.5	Max 5 ms pulse	-	(Reddy et al. 2019)
GaN-Si	50 (diameter)	460	300 × 300	0.090	5	Si	1	-	15	1	Below 1 mA currents	Mice, hippocampus	(Yasunaga et al. 2022)
GaN-Sa transferred to PI	50 × 50 × 6.45	-	300 × 20	0.0060	4	PI	-	-	40	1.5	Below 20 Hz	Mice, VTA	(Il Kim et al. 2013)
GaN-Sa transferred to PI	125 × 180	480/630	320 × 120	0.038	1	PI	3/10	-	60/45	8.0/4.0	Below 3 mA currents/Below 30 Hz up to 10 mA	Mice, VTA	(Li et al. 2022)
GaN-Sa transferred to Si	100 (diameter)	455	150 × 65	-	10	Si	5	0.450	56	2.0	Below 3 mA currents and 500 ms pulses	Mice, cortex S1	(Ayub et al. 2020)
GaN-Sa	250 × 490	444	400 × 200	0.080	1	Sa	35	-	5	-	-	-	(Shen et al. 2022)
GaN-Sa	40 (diameter)	450	80 × 101	0.0081	5	Sa	0.1	-	10	-	Below 50 Hz	-	(McAlinden et al. 2013)
Commercial flip chip LED	220 × 270 × 50	470	350 × 130	0.045	1	PI	5	-	50	-	Below 60% duty cycles	Mic, Nac/VTA	(Shin et al. 2017)
Commercial flip chip LED	220 × 270 × 50	460	250 × 60	0.016	3	PI	10	0.5	10	1.7	-	Mice, nRT	(Ayub et al. 2017)

Table 1 (continued)

µLED	µLED dimensions (w x l x h) (µm)	µLED emission peak (nm)	Probe shank dimensions (w x h) (µm)	Cross-sectional area (mm^2)	µLEDs per shank	Probe substrate	Safe* max working current (mA)	Optical power at safe* current (mW)	Irrandiance at safe* current (mW/mm^2)	Peak Wall-plug efficiency (%)	Temperature below 1 ºC	In vivo testing	Ref
Commercial flip chip LED	220 × 270 × 50	465/540	650 × 700	0.45	2	PDMS	-	-	12	-	Below 70% duty cycles	Mice, Nac	(Il Park et al. 2016)
Commercial flip chip LED	290 × 550 × 100	455	900 × 500	0.45	1	PCD	-	-	1.55	-	Below 1 Hz and 100 ms pulses	Rat, V1	(Fan et al. 2016)

Abbreviations: *CA1* hippocampus cornus ammonis 1, *GaN* gallium nitride, *M1* primary motor cortex, *nRT* nucleus reticularis thalami, *PCD* polycrystalline diamond, *PDMS* Polydimethylsiloxane, *PI* polyimide, *SI* primary somatosensory cortex, *Sa* sapphire, *Si* silicon, *VTA* ventral tegmental area

*Safe working current or voltage were defined as the current or voltage values that do not lead to increases over 1 ºC in probe hotspot temperature or brain tissue with the most conservative driving parameters; if temperature assessment was not provided, the maximum working current is reported (when available)

and the optical coating were considered in the model. The µLED heating was assumed to be due to the dissipated power corresponding to the difference in input electrical power and output optical power. The heating of the brain due to optical absorption of the emitted light was assumed to be negligible. Several simulations were ran for all possible combinations of the following stimulation driving parameters: 2.7, 2.8, and 2.9 V (0.75, 1.3, and 2 mA, respectively), 10 and 20 Hz frequency, and 20, 50, and 80% duty cycles (Fig. 4d). The observed induced temperature changes in the brain tissue close to the µLED were dependent on the µLED driving parameters, with higher voltages, lower frequencies, and longer duty cycles inducing the highest temperature rises. The longer the µLED was turned on at each driving voltage (i.e. lower frequencies and/or longer duty cycles) the higher the heating, as previously reported for other neural probes (Wu et al. 2015; Scharf et al. 2016; Ayub et al. 2020; Il Kim et al. 2013; Shin et al. 2017). From the tested driving parameters, all possible combinations with 20% duty cycles (except 2.9 V at 10 Hz) lead to brain tissue temperature rises below 1 ºC. With 50% and 80% duty cycles, only voltages below 2.7 V (0.75 mA) did not raise brain tissue temperature above the safe limit of 1 ºC. Using these lower input power settings, an irradiance of approximately 40 mW/mm^2 is expected, which well above the threshold of 1 mW/mm^2necessary for channelrhodopsin activation (Grossman et al. 2011).

Compared with previously reported µLED neural probes, our probe presents lower heating for similar driving power (Table 1). This can be partly explained by the significantly higher WPE of the µLED used and the potential reduction of the hotspot temperature through heat blocking by the 10 µm optical acrylic passivation coating which has low thermal conductivity and can block heat transfer. A modeling study estimated that µLED hotspot temperatures on neural probes can decrease by 50% with only 20 µm of encapsulation (Dong et al. 2018). The heating of brain tissue through µLED operation is also likely lower than modeled because of the large heat capacity of brain tissue that prevents significant temperature elevations. Blood flow in the brain's vasculature works as an active heatsink that contributes to actively modulate brain temperature (Sukstanskii and Yablonskiy 2006). Previous studies support that temperature elevations in the tissue will be even lower than those measured or modeled at neural probe's surface (Wu et al. 2015; McAlinden et al. 2013; Yasunaga et al. 2022). Heat dissipation through metal interconnect lines, working as temporary heat buffers due to their high thermal conductivity, can also contribute to reduce µLED's hotspot temperature in neural probes (Scharf et al. 2016; Reddy et al. 2019; Dong et al. 2018; McAlinden et al. 2013). Previous reports showed that relevant heat dissipation in µLED probes can

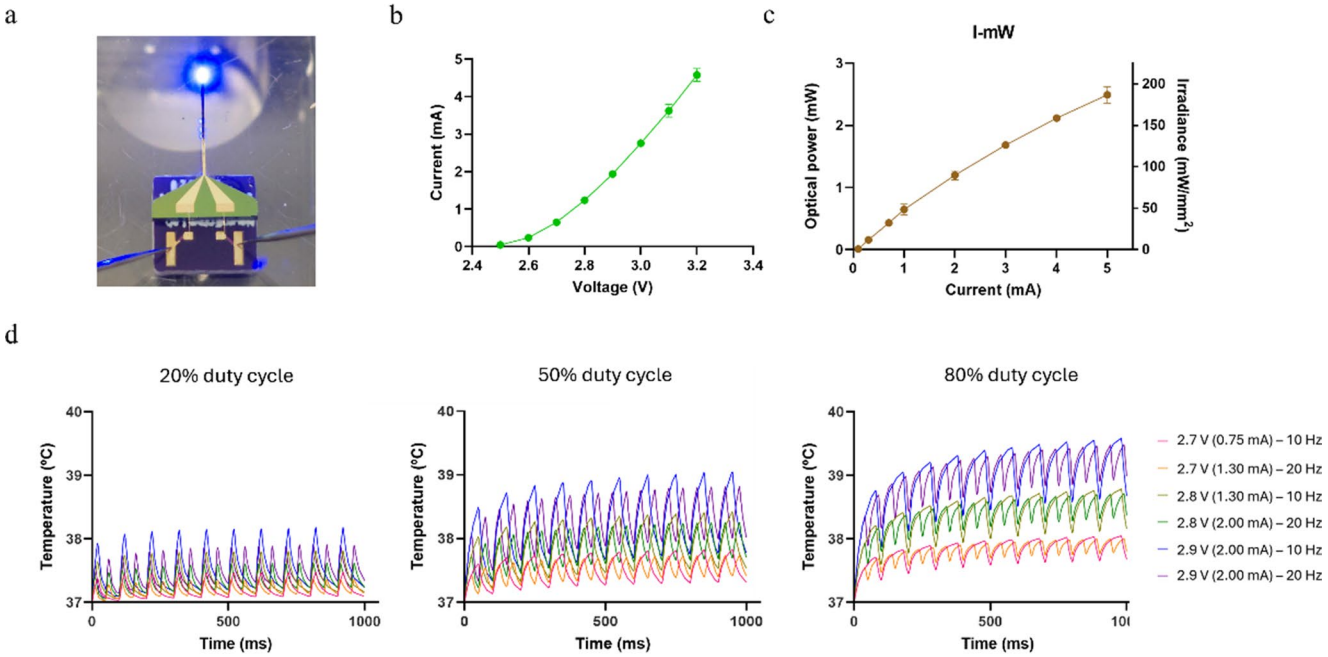

Fig. 4 Opto-electrical and thermal modeling of neural probes with µLED. (**a**) Photograph of probe wire-bonded to the PCB and driven by tungsten needles from probe station. (**b**) Representative I-V curve (n = 4, error bars are s.d.). (**c**) Representative optical power and irradiance of neural probe with µLED as a function of driving current (n = 3, error bars are s.d.). (**d**) Simulation of brain tissue temperature modulation, based on COMSOL thermal modeling, for µLED pulsed operation (10 and 20 Hz) for different driving voltages (2.7, 2.8, and 2.9 V) and duty cycles (20%, 50%, and 80%; left, middle, and right panels, respectively) during 1 s

occur through metal lines and can even lead to considerable hotspot temperature elevations in the exposed electrode sites of probes combining capacitive metal electrodes with µLEDs (Reddy et al. 2019; Dong et al. 2018). However, the gold interconnect lines in our probe were not included in the simulation model because adding a nanometric layer would increase the the required computing power significantly. Therefore, it cannot be discard that a portion of heat dissipation likely occurred through the interconnect lines due to the high thermal conductivity of gold potentially leading to lower µLED's hotspot temperature during operation.

3.4 In vivo testing

Before in vivo testing in mice, the longevity of the µLED optical coating encapsulation was assessed. The shank of a neural probe was immersed in phosphate-buffered saline (PBS) continuously for 12 days, and current measurements at 2.8 V were taken every 24 h (Fig. 5a). A current of approximately 1.30 mA was measured every day (Fig. 5a), confirming that the regular operation of the probe was maintained even in continuous immersion in liquid solution. The process of immersing µLED probes in PBS was repeated with another 5 randomly chosen neural probes for different durations (5–12 days) but current measurements were not taken. Functioning of the probes was only visually confirmed by driving them with different voltages (2.7 to 3.2 V) in PBS at the end of the defined immersion period. All tested probes were fully functional after prolonged immersion.

To assess the in vivo performance of the µLED neural probe, a custom tetrode device (Machado et al. 2020) carrying 4 nichrome tetrodes was combined with a µLED probe for simultaneous optical stimulation and electrophysiological activity recordings (Fig. 5b). One anesthetized Emx1-cre:Ai27D mouse expressing channelrhodopsin in brain cortical neurons was acutely implanted with the tetrodes-µLED probe assembly in the primary motor cortex (M1). Pulsed brain illumination through the µLED at 2.75 V (approximately 1 mA) reliably induced spiking activity across all trials (Fig. 5b). On each trial, the multi-unit activity (MUA) spike rate increased from below 1 Hz to over 25 Hz, confirming strong neuronal activation with optical stimulation. The capability of the neural probe to drive neuronal activity when implanted inside the brain was only tested in one anesthetized animal, and further tests with chronic implants in freely moving mice will be needed to analyze its application in neuroscience behavioral experiments.

4 Conclusion

In contrast to previous µLED neural probes with monolithically integrated or transfer-printed LEDs with low quantum efficiency and low output power or commercial bare

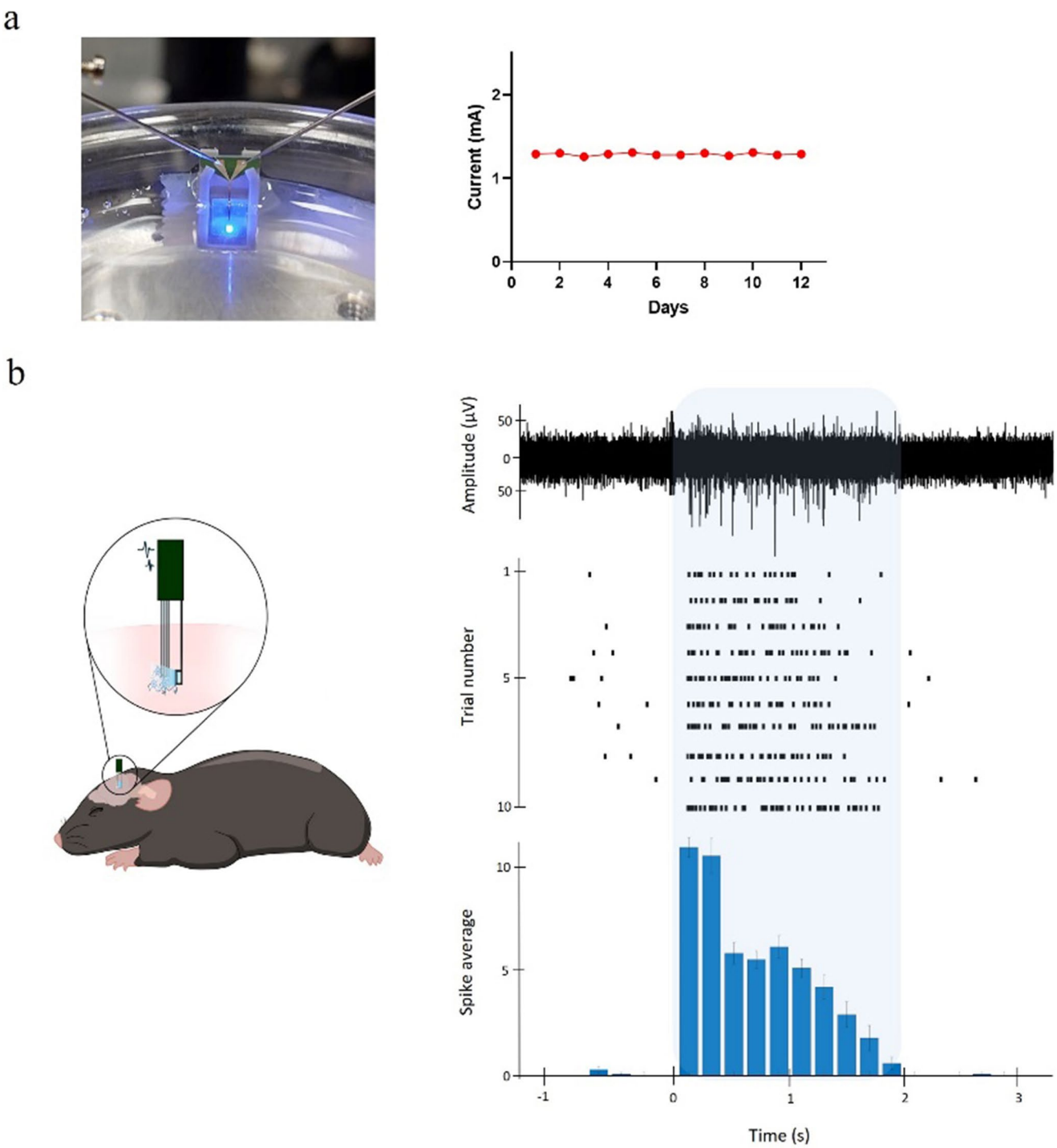

Fig. 5 Passivation and in vivo testing. (**a**) Neural probe submerged in phosphate-buffered saline (PBS) with needles from probe station driving µLED to emit light (left). Current measured daily at 2.8 V during 12 days of continuous immersion in PBS (right). (**b**) Cartoon of tetrode device and neural probe with µLED assembly implanted in mouse's motor cortex (M1) for simultaneous electrophysiological recordings and optical stimulation (left). Raw trace (bandpass filtered 300–3000 Hz) of one optical stimulation trial with electrophysiological activity before, during and after optical stimulation (righ, top). Raster plot of spikes detected in 10 optical stimulation trials (right, center). Cumulative peri-stimulus time histogram (PSTH) with total spike count across all optical stimulation trials (right, bottom). Blue shaded area corresponds to optical stimulation period. Bins in PSTH are 200 ms

LED chip bonding on thick substrates, we have designed a novel process to integrate low-cost and highly efficient LED chips in neural probes with reduced thickness (15 µm). This approach created small form factor implantable neural probes with a cross-section lower than that found in the smallest optical fibers used for in vivo optogenetic studies and with high optical output power with relatively low operating power/current. In vivo validation with simultaneous electrophysiological recordings confirmed that our neural probe can reliably induce strong spiking activity in neuronal populations expressing channelrhodopsin.

Supplementary Information The online version contains supplementary material available at https://doi.org/10.1007/s10544-025-00754-1.

Acknowledgements The authors would like to thank Helder Fonseca and José Fernandes of INL for assistance with the HF etching process, as well as all members of the Neurophysiology and Neuroengineering Lab at FMUP and the Alpuim group (former 2D Materials and Devices group) at INL for discussions on probe design and fabrication processes.

Author contributions MA and TP designed the probe layout. MA fabricated the probe, with assistance from JB. TP and JB developed the µLED mounting process. PS designed the interface PCBs and performed probe characterization measurement with TP. TP performed thermal modelling simulations. MF and PS performed in vivo testing. PS and LJ analyzed electrophysiological recordings. MA, TP, PS, and LJ wrote the first draft of the manuscript. PA and LJ revised the manuscript, acquired funding, and supervised work. All authors read and approved the final version of the manuscript.

Funding Open access funding provided by FCT|FCCN (b-on).
This work was supported by "la Caixa" Banking Foundation under grant agreement LCF/PR/HR21-00410. MA and MF were supported by Portuguese Foundation for Science and Technology (FCT) doctoral fellowships 2022.14536.BD and 2023.00604.BD, respectively.

Data availability All data supporting the findings of this study are available in the paper and its Supplementary Information section.

Declarations

Ethics approval All procedures involving animals were conducted in accordance with European Union Directive 2016/63/EU and the Portuguese law on the protection of animals for scientific purposes (DL No 113/2013), and approved by the Portuguese National Authority for Animal Health and the Animal Welfare Committee at FMUP (ORBEA-FMUP).

Competing interests The authors declare no competing interests.

References

S. Ayub et al., Hybrid intracerebral probe with integrated bare LED chips for optogenetic studies. Biomed. Microdevices. (2017). https://doi.org/10.1007/s10544-017-0190-3

S. Ayub et al., Compact optical neural probes with up to 20 integrated Thin-Film leds applied in acute optogenetic studies. IEEE Trans. Biomed. Eng. (2020). https://doi.org/10.1109/TBME.2020.2966293

B.J. Barros, J.P.S. Cunha, Neurophotonics: a comprehensive review, current challenges and future trends. Front. Neurosci. **18** (2024). https://doi.org/10.3389/fnins.2024.1382341

J.G. Bernstein, E.S. Boyden, Optogenetic tools for analyzing the neural circuits of behavior. Trends Cogn. Sci. (2011). https://doi.org/10.1016/j.tics.2011.10.003

W. Chen et al., The roles of optogenetics and technology in neurobiology: A review. Front. Aging Neurosci. (2022). https://doi.org/10.3389/fnagi.2022.867863

J. Chen, H. Ding, X. Sheng, Advanced manufacturing of microscale light-emitting diodes and their use in displays and biomedicine. J. Inf. Disp. (2024). https://doi.org/10.1080/15980316.2023.2248403

K. Deisseroth, Circuit dynamics of adaptive and maladaptive behaviour. Nature. (2014). https://doi.org/10.1038/nature12982

N. Dong et al., Opto-electro-thermal optimization of photonic probes for optogenetic neural stimulation. J. Biophotonics. (2018). https://doi.org/10.1002/jbio.201700358

B. Fan, K.-Y. Kwon, R. Rechenberg, M.F. Becker, A.J. Weber, W. Li, A hybrid neural interface optrode with a polycrystalline diamond heat spreader for optogenetics. TECHNOLOGY. (2016). https://doi.org/10.1142/s2339547816400021

L. Fenno, O. Yizhar, K. Deisseroth, The development and application of optogenetics. Annu. Rev. Neurosci. (2011). https://doi.org/10.1146/annurev-neuro-061010-113817

S.B. Goncalves, J.F. Ribeiro, A.F. Silva, R.M. Costa, J.H. Correia, Design and manufacturing challenges of optogenetic neural interfaces: A review. J. Neural Eng. (2017). https://doi.org/10.1088/1741-2552/aa7004

J.A. Gorski, T. Talley, M. Qiu, L. Puelles, J.L.R. Rubenstein, K.R. Jones, Cortical excitatory neurons and glia, but not GABAergic neurons, are produced in the Emx1-expressing lineage. J. Neurosci. **22**(15), 6309–6314 (2002). https://doi.org/10.1523/jneurosci.22-15-06309.2002

N. Grossman, K. Nikolic, C. Toumazou, P. Degenaar, Modeling study of the light stimulation of a neuron cell with channelrhodopsin-2 mutants. IEEE Trans. Biomed. Eng. (2011). https://doi.org/10.1109/TBME.2011.2114883

M. HajjHassan, V. Chodavarapu, S. Musallam, NeuroMEMS: neural probe microtechnologies. Sensors. (2008). https://doi.org/10.3390/s8106704

T. Il Kim et al., Injectable, cellular-scale optoelectronics with applications for wireless optogenetics. Sci. (80-). (2013). https://doi.org/10.1126/science.1232437

S. Il Park et al., Stretchable multichannel antennas in soft wireless optoelectronic implants for optogenetics. Proc. Natl. Acad. Sci. U. S. A. (2016) https://doi.org/10.1073/pnas.1611769113

L. Li et al., Colocalized, bidirectional optogenetic modulations in freely behaving mice with a wireless dual-color optoelectronic

probe. Nat. Commun. (2022). https://doi.org/10.1038/s41467-022-28539-7
F. Machado, N. Sousa, P. Monteiro, L. Jacinto, A versatile and modular tetrode-based device for single-unit recordings in rodent ex vivo and in vivo acute preparations. J. Neurosci. Methods **341** (2020). https://doi.org/10.1016/j.jneumeth.2020.108755
L. Madisen et al., A toolbox of Cre-dependent optogenetic Transgenic mice for light-induced activation and Silencing. Nat. Neurosci. **15**(5), 793–802 (2012). https://doi.org/10.1038/nn.3078
N. McAlinden et al., Thermal and optical characterization of micro-LED probes for in vivo optogenetic neural stimulation. Opt. Lett. (2013). https://doi.org/10.1364/ol.38.000992
J.P. Newman et al., Twister3: a simple and fast microwire twister. J. Neural Eng. (2020). https://doi.org/10.1088/1741-2552/ab77fa
A. Novais et al., Hybrid multisite silicon neural probe with integrated flexible connector for interchangeable packaging. Sensors **21**(8) (2021). https://doi.org/10.3390/s21082605
S.F. Owen, M.H. Liu, A.C. Kreitzer, Thermal constraints on in vivo optogenetic manipulations. Nat. Neurosci. (2019). https://doi.org/10.1038/s41593-019-0422-3
R. Qazi, C.Y. Kim, S.H. Byun, J.W. Jeong, Microscale inorganic LED based wireless neural systems for chronic in vivo optogenetics. Front. NeuroSci. (2018). https://doi.org/10.3389/fnins.2018.00764
J.W. Reddy et al., High density, double-sided, flexible optoelectronic neural probes with embedded μLEDs. Front. Genet. **10**(JUL) (2019). https://doi.org/10.3389/fnins.2019.00745
R. Scharf, T. Tsunematsu, N. McAlinden, M.D. Dawson, S. Sakata, K. Mathieson, Depth-specific optogenetic control in vivo with a scalable, high-density MlED neural probe. Sci. Rep. (2016). https://doi.org/10.1038/srep28381
J. Shen et al., Double-Sided Sapphire optrodes with conductive shielding layers to reduce optogenetic stimulation artifacts. Micromachines. (2022). https://doi.org/10.3390/mi13111836
G. Shin et al., Flexible Near-Field wireless optoelectronics as subdermal implants for broad applications in optogenetics. Neuron. (2017). https://doi.org/10.1016/j.neuron.2016.12.031
J.H. Siegle, A.C. López, Y.A. Patel, K. Abramov, S. Ohayon, J. Voigts, Open Ephys: an open-source, plugin-based platform for multi-channel electrophysiology. J. Neural Eng. **14**(4) (2017). https://doi.org/10.1088/1741-2552/aa5eea
P. Silva, L. Jacinto, Wireless devices for optical brain stimulation: a review of current developments for optogenetic applications in freely moving mice. Cell. Mol. Bioeng. **18**(1), 1–13 (2025). https://doi.org/10.1007/s12195-024-00832-z
A.L. Sukstanskii, D.A. Yablonskiy, Theoretical model of temperature regulation in the brain during changes in functional activity. Proc. Natl. Acad. Sci. U. S. A. (2006) https://doi.org/10.1073/pnas.0604376103
H.K. Sung, H.K. Lee, C. Wang, N.Y. Kim, Design and fabrication of implantable neural probes with monolithically integrated light-emitting diodes for optogenetic applications. J. Nanosci. Nanotechnol. (2017). https://doi.org/10.1166/jnn.2017.13071
K.M. Tye, K. Deisseroth, Optogenetic investigation of neural circuits underlying brain disease in animal models. Nat. Rev. Neurosci. (2012). https://doi.org/10.1038/nrn3171
M.R. Warden, J.A. Cardin, K. Deisseroth, Optical neural interfaces. Annu. Rev. Biomed. Eng. (2014). https://doi.org/10.1146/annurev-bioeng-071813-104733
F. Wu, E. Stark, P.C. Ku, K.D. Wise, G. Buzsáki, E. Yoon, Monolithically integrated MLEDs on silicon neural probes for High-Resolution optogenetic studies in behaving animals. Neuron. (2015). https://doi.org/10.1016/j.neuron.2015.10.032
S. Xu et al., Illuminating the brain: advances and perspectives in optoelectronics for neural activity monitoring and modulation. Adv. Mater. (2023). https://doi.org/10.1002/adma.202303267
H. Yasunaga et al., MicroLED neural probe for effective in vivo optogenetic stimulation. Opt. Express. (2022). https://doi.org/10.1364/oe.470318
O. Yizhar, L.E. Fenno, T.J. Davidson, M. Mogri, K. Deisseroth, Optogenetics in neural systems. Neuron. (2011). https://doi.org/10.1016/j.neuron.2011.06.004
H. Zeng, L. Madisen, Mouse transgenic approaches in optogenetics. Progr. Brain Res. (2012). https://doi.org/10.1016/B978-0-444-59426-6.00010-0